PCCP

Accepted Manuscript

ROYAL SOCIETY OF CHEMISTRY

www.rsc.org/pccp

Graphical Abstract

Zn doping was proved to be helpful in stabilizing the crystal structure of $Li_3V_2(PO_4)_3$/C upon repeated cycles.

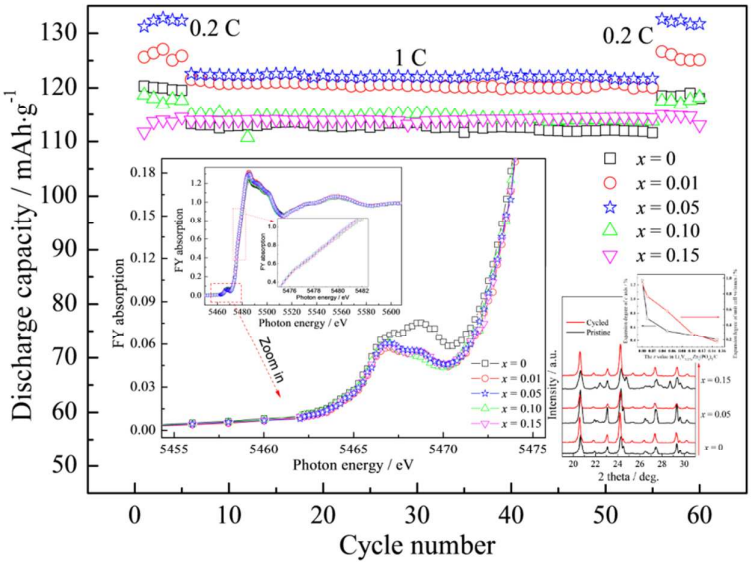

Physical Chemistry Chemical Physics

Cite this: DOI: 10.1039/c0xx00000x

www.rsc.org/xxxxxx

ARTICLE TYPE

Enhancement of cycling performance of $Li_3V_2(PO_4)_3$/C by stabilizing the crystal structure through Zn^{2+} doping

Wenhui Wang,[a]† Jiaolong Zhang,[a]† Zheng Jia,[a] Changsong Dai,[*a] Yongfeng Hu,[b] Jigang Zhou[b] and Qunfeng Xiao[b]

Received (in XXX, XXX) Xth XXXXXXXXX 20XX, Accepted Xth XXXXXXXXX 20XX
DOI: 10.1039/b000000x

A series of $Li_3V_{2-2/3x}Zn_x(PO_4)_3$/C were synthesized by carbon thermal reduction assisted with ball-mill process. Scanning electron micrograph (SEM) shows that the irregular morphology of the pristine $Li_3V_2(PO_4)_3$/C can be transformed to spherical upon doping with the suitable amount of zinc. The structural stability of the pristine and the Zn doped $Li_3V_2(PO_4)_3$/C were investigated *via* X-ray absorption near edge structure (XANES) and X-ray diffraction (XRD). The results reveal that Zn doping not only improves the stability of VO_6 octahedra structure before electrochemical cycling, but also reduces the irreversible expansion degree of the *c* axis as well as crystal volumes upon repeated cycles. Among $Li_3V_{2-2/3x}Zn_x(PO_4)_3$/C ($0 \le x \le 0.15$) series, the 0.05 Zn per formula unit doped sample shows the best electrochemical performance. Excess Zn doping ($x > 0.05$) didn't result in further improvement in electrochemical performance due to the segregation effect and the non-active nature of Zn.

Introduction

Although lithium ion batteries (LIBs) have gained largest market shares in consumer electronics due to their relatively high energy density, their extensive application in electric vehicles (EVs) and/or hybrid electric vehicles (HEVs) is still very challenging and limited. To revolutionize the transportation technology by reducing the dependence on fossil oil and decreasing the carbon footprint [1], intensive studies are focusing on higher energy density and safety of cathode materials. In the intensive search, lithium vanadium phosphate ($Li_3V_2(PO_4)_3$, LVP) has emerged as one of the most promising materials for a long time, due to its extraordinary high-rate performance [2], high energy density (discharge capacity × operating voltage) [3-6] and excellent low temperature performance [7]. Generally, LVP is believed to suffer most from the low electric conductivity [8]. Therefore, too much attentions have been attracted and many approaches have been proposed to solve this problem by: (1) preparing nano-sized particles [9], (2) coating with a conductive thin film such as carbon [10], oxides [11] and/or metals [12], (3) morphology control [13-17] and/or (4) metal ion doping (*i.e.* Nb, Fe, Al, K, Mg, Ca, Sc, Na, Ni, Cl, etc.) [18-24]. However, important also is the long service life of the LIBs [25], which always not fully discussed or even don't discussed in the previous literatures, for the potential mass market of EVs. Thus, we herein focus on the enhancement of structural stability of LVP during charge/discharge process, which one of the most important factor responsible for the long calendar life.

Although zinc doping was proved to be effective in improving the electrochemical performance of $LiFePO_4$ [26, 27], the effect on the electrochemical and structural properties of LVP has not been studied, especially its functioning mechanism. X-ray absorption near edge structure (XANES) spectroscopy probes the modulation of the absorption coefficient above a particular edge of an interested element [28] and is a powerful method to study local structure [29] in terms of the electronic and chemical information. In this paper, possible mechanisms of Zn doping in LVP were proposed based on the XANES spectroscopy at Li K-edge, V K-edge, P L-edge and the crystal evolution of the selected samples upon repeating cycles, which agrees with the evolution of the electrochemical performance of $Li_3V_{2-2/3x}Zn_x(PO_4)_3$/C ($x = 0$, 0.01, 0.05, 0.10, and 0.15) series.

Experimental

Synthesis and characterization of samples

Typically, the LVP/C sample was prepared using $LiOH{\cdot}H_2O$ (A.R.), V_2O_5 (A.R.), $NH_4H_2PO_4$ (A.R.) and sucrose at a molar ratio of 3:1:3:2/3. During the preparation, the added sucrose was transformed to carbon which can not only reduce V^{5+} to V^{3+} but also form a continuous carbon network for electrical conduction. These raw materials were first ball-milled together for 7 h with absolute ethanol as dispersant. The obtained mixture was heated to 300 °C under an argon atmosphere for 4 h to expel NH_3, H_2O, etc. Then, the mixture was ground and heated to 800 °C under a reducing atmosphere for 8 h. The product was ground in an agate mortar for later use.

For the Zn-doped samples, the procedures were the same as those for LVP/C except a stoichiometric amount of $(CH_3COO)_2Zn{\cdot}2H_2O$ (A.R.) was added.

The crystal structures of the samples were carefully examined before and after cycling in the potential range of 3.0-4.3 V with XRD using a D/max-γB X-ray diffractometer (Rigaku, Japan) with Cu Kα radiation (λ= 0.154178 nm), a voltage of 45 kV, a current of 50 mA, a scan rate of 4°□min^{-1} and 2θ from 10 to 70°. The morphology and particle sizes of the samples were observed with a scanning electron microscope (SEM, HITACHI S-4700, Japan). V K-edge, P L-edge and Li K-edge X-ray absorption near

edge structure (XANES) spectroscopy were conducted at the CLS using SXRMB and VLS-PGM beamlines. The powder sample was mounted on the double-sided, conducting carbon tape. XANES was recorded in the surface sensitive total electron yield (TEY) or fluorescence yield (FY) using a silicon drift detector (SDD) at SXRMB and a micro-channel plate (MCP) detector at PGM. XANES data was first normalized to the incident photon flux I_0, and then normalized to the edge jump as unity.

Assembly of cells and electrochemical measurements

The cathode slurry was prepared by mixing the LVP/C with acetylene black and polyvinylidene fluoride (PVDF) at a mass ratio of 80:10:10 in *n*-methyl-2-pyrrolidone (NMP). Then, aluminum foils with a thickness of 20 μm were coated with the cathode slurry. The coated Al foils were roll-pressed at a pressure of 5 MPa after being dried at 110 °C under vacuum for 12 h and then cut into wafers (15 mm in diameter) as cathode sheets. A typical cathode sheet was 8.5–9.5 mg in weight and 0.1 mm thick. The anodes were lithium foils of about 0.30 mm thick. Celgard 2400 with a thickness of about 0.02 mm was used as the separator. 1M $LiPF_6$ in a mixture of ethylene carbonate (EC), dimethyl carbonate (DMC) and diethyl carbonate (DEC) (a volume ratio of 1:1:1) was used as the electrolyte. CR2025-type coin cells were assembled in a glove box filled with high-purity argon.

The coin cells were galvanostatically charged/discharged at different rates over the potential range of 3.0~4.3 V using a multichannel battery test system (Neware, Shenzhen). CHI-750d was also used in the electrochemical impedance spectroscopy (EIS) test over a frequency range from 10 mHz to 10 kHz by applying an AC signal of 5 mV. All experiments were carried out at a temperature of 25±0.5 °C.

Results and discussion

Sample characterization

XRD analyses were conducted to examine the crystal structure of $Li_3V_{2-2/3x}Zn_x(PO_4)_3$/C ($x$ = 0, 0.01, 0.05, 0.10 and 0.15) series. For $0 \le x \le 0.10$, the prepared compositions show a single monoclinic structure with no observable diffraction peaks due to impurity, while some miscellaneous phases were observed for x = 0.15. Detailed analysis of phase shows that the impurity phases are Li_2ZnO_2 (denoted by diamonds), $Zn_2V_2O_7$ (denoted by arrows) and $Zn_2P_2O_7$ (denoted by spade), which may be ascribed to ejection of some zinc from the monoclinic structure forming these minor phases at high substitution level. Based on the XRD patterns, no additional carbon-related diffraction peak is detected, which indicates that the residual carbon yielded from pyrolysis of sucrose is amorphous and/or the residual carbon layer on the LVP/C particles was too thin to be detected.

The lattice parameters and the unit cell volumes of $Li_3V_{2-2/3x}Zn_x(PO_4)_3$/C were obtained from least square refinement based on a monoclinic structure, and the results are summarized in Table 1. The unit cell volume increase with the substitution of V^{3+} (0.078 nm) [8] site by larger Zn^{2+} (0.083 nm) [26], indicating the successful doping of partial or full Zn into the LVP/C crystal lattice. The expansion in unit cell volume could facilitate the extraction/reinsertion of lithium ions.

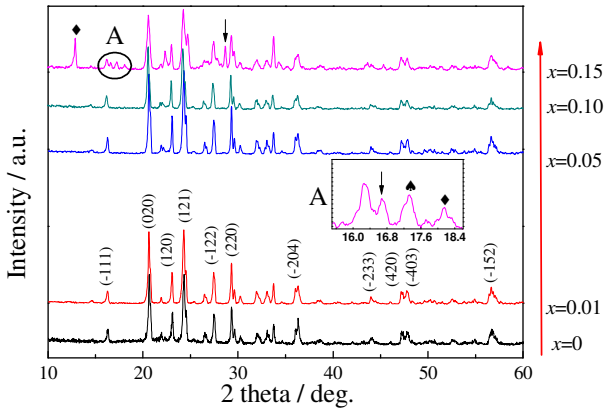

Fig.1 XRD patterns of $Li_3V_{2-2/3x}Zn_x(PO_4)_3$/C samples

Table 1 Cell parameters of $Li_3V_{2-2/3x}Zn_x(PO_4)_3$/C samples

x	a / nm	b / nm	c / nm	β	V / nm^3
0	0.8634(8)	0.8592(2)	1.20446(6)	90.0564	0.8936(2)
0.01	0.8614(5)	0.8598(6)	1.21010(5)	90.2318	0.8963(5)
0.05	0.8627(0)	0.8602(0)	1.20952(7)	90.3018	0.8975(8)
0.10	0.8620(8)	0.8611(8)	1.21094(2)	90.0266	0.8990(1)
0.15	0.8634(1)	0.8589(2)	1.21356(4)	90.3162	0.8999(7)

The SEM images and the corresponding particle size distribution histogram are shown in Fig.2 presenting the morphological properties of the samples. As can be seen in the SEM images, the addition of Zn has remarkable influence on the morphology of samples. The doped samples were transformed to spherical shapes from irregular shapes of pristine sample, with severe agglomeration phenomenon emerged for x = 0.15. The morphological transformation to spherical kind, but before severe agglomeration, would favor the improvement of the electrochemical properties. On one hand, the high specific areas of spherical morphology increase the contact areas with the electrolytes, thus could improve the electrochemical reactivity; On the other hand, the space between the spherical particles allows better penetration of the electrolyte, which could shorten the distance for the extraction/reinsertion of lithium ions; Moreover, the spherical particles facilitate a more orderly accumulation, thereby effectively improving the tap density of the samples.

The particle size distribution (PSD) histogram shows all the samples having a narrow size distribution ranging from 0.1 μm to 1.5 μm. Normal distribution fitting shows a negative correlation between the average particle size and the doping amount of Zn for $0 \le x \le 0.05$, but a positive correlation between them for $0.10 \le x \le 0.15$, which seems somewhat incomprehensible. However, upon careful observation of the SEM images, we found the increase of particle size at high substitution level can be ascribed to the agglomeration of the primary particles. This led us to conclude that the Zn doping does reduce the primary particle size of the sample, but the increased surface energy for the much smaller particle would aggregate to form secondary particles at

Physical Chemistry Chemical Physics

Cite this: DOI: 10.1039/c0xx00000x

www.rsc.org/xxxxxx

ΑΡΤΙΧΛΕ ΤΥΠΕ

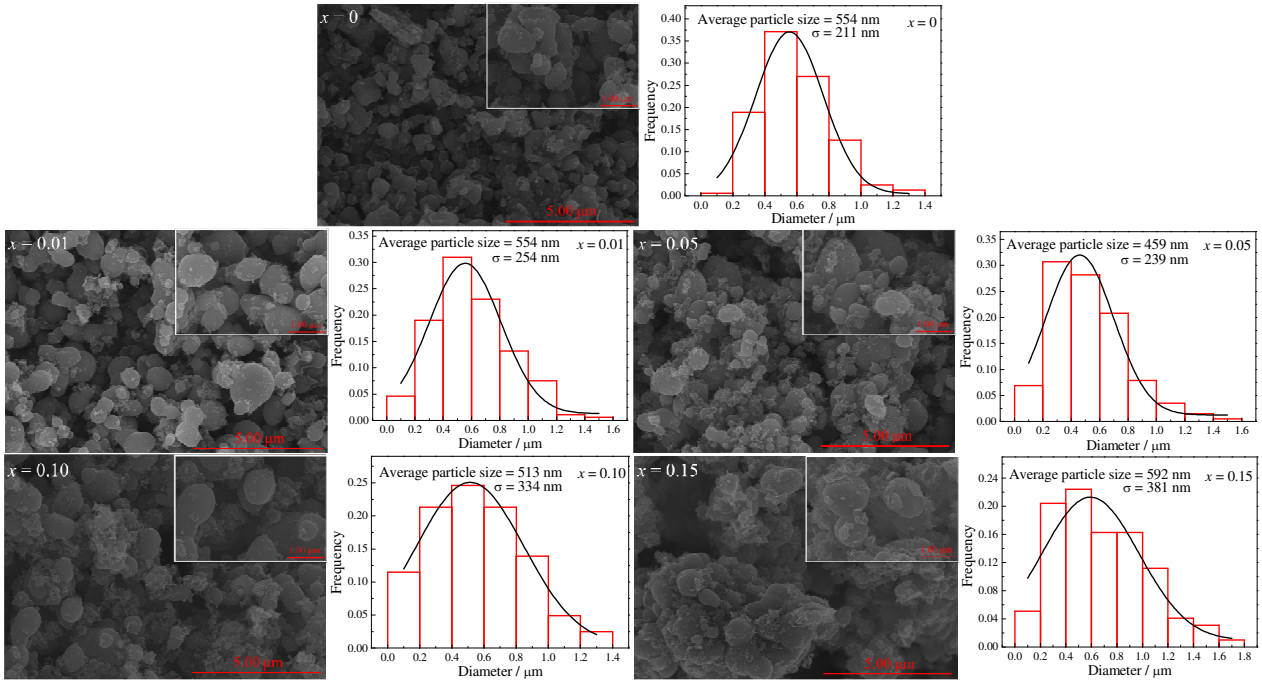

Fig.2 (a) SEM images and (b) the corresponding particle size distribution histogram of $Li_3V_{2-2/3x}Zn_x(PO_4)_3$/C samples

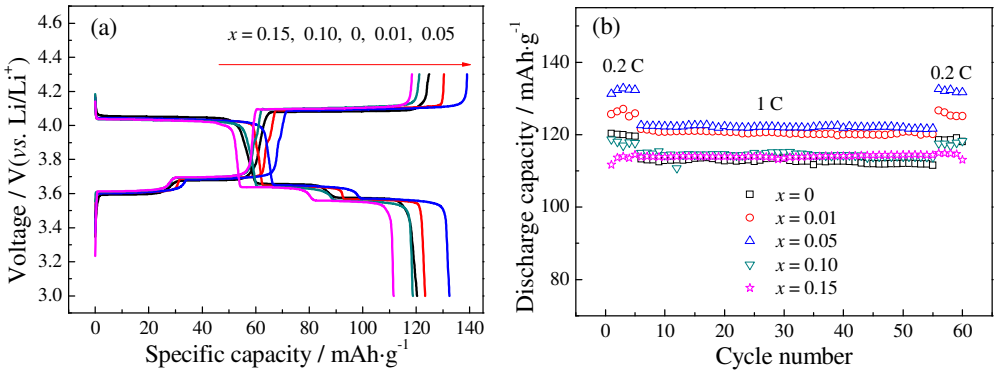

Fig.3 (a) Initial charge/discharge curves at 0.2 C rates and (b) cycle performance of $Li_3V_{2-2/3x}Zn_x(PO_4)_3$/C samples

Table 2 The initial discharge capacities and capacity retention rates after 50 cycles of $Li_3V_{2-2/3x}Zn_x(PO_4)_3$/C samples at different rates for Fig. 3b

Samples	0.2 C 1st (mAh g^{-1})	1 C		0.2 C 1st (mAh g^{-1})
		1st (mAh g^{-1})	50th/1st	
0	120.3	113.3	98.4%	111.5
0.01	125.6	121.5	98.8%	120.0
0.05	131.2	122.6	99.3%	121.7
0.10	118.7	114.9	99.1%	113.7
0.15	111.7	113.9	100%	114.4

the action of the higher surface energy. In addition, the relationship between the uniformity of PSD and the amount of dopant is similar to that of the average particle size, *i.e.*,0.05 Zn doped sample have the most uniform particle size relative to other doping samples.

Electrochemical measurements

A constant-current charge/discharge test was carried out to characterize the effect of zinc doping on electrochemical performances of the samples, and the results were presented in Fig.3. For $Li_3V_{2-2/3x}Zn_x(PO_4)_3$/C samples, three couple of plateaus can be observed from the initial charge/discharge curves at 0.2 C (1 C = 133 mA g^{-1}) rates (Fig.3b), which could be assigned to a sequence of phase transitions of $Li_yV_{2-2/3x}Zn_x(PO_4)_3$/C ($y$ = 3.0, 2.5, 2.0, 1.0). And desirable symmetrical shapes between the charge and discharge curves of the $Li_3V_{2-2/3x}Zn_x(PO_4)_3$/C series were obtained, which indicate a good reversibility of the extraction/reinsertion of the first two Li^+ ions.

The cycle performances of the samples are presented in Fig.3b and the corresponding retentions rates are also listed in Table 2. Due to the beneficial effect of the suitable amount of zinc doping, $Li_3V_{1.97}Zn_{0.05}(PO_4)_3$/C shows the best electrochemical performance in $Li_3V_{2-2/3x}Zn_x(PO_4)_3$/C series: the initial discharge capacity of $Li_3V_{1.97}Zn_{0.05}(PO_4)_3$/C is 131.2 mAh g^{-1} at 0.2 C rates, when operated at 1 C rate, the discharge capacities for 1^{st} and 50^{th} cycle are 122.6 and 121.7 mAh g^{-1}, respectively. After 55 cycles, the electrode still delivers a discharge capacity of 132.6 mAh g^{-1} when reset to 0.2 C charge/discharge rates, which is as high as the initial discharge capacity. However, excessive amount of zinc doping ($x \geq 0.10$) led to a decrease of specific discharge capacity since Zn is electrochemically inactive in the potential range of 3.0-4.3 V. More interestingly, the capacity retention rate gradually increases, on the whole, with the increase of the amount of dopant up to x = 0.05. While the oxidation of V^{3+}, as a result of the extraction of lithium-ion during charge process, would cause shrinking of the crystal lattice or even the collapsing of the local structure, the unchangeable radius of Zn^{2+} dopant [26] could be regarded as a stabilizer in preventing local structural collapse during charge/discharge processes, thus enhancing the cycle performance of LVP/C. To put in a nutshell, we speculate that the improvement of the cycling performance is mainly due to the enhanced structural stability of samples through Zn^{2+} doping.

To prove the proposed hypothesis, we choose to study the oxidation states of $Li_3V_{2-2/3x}Zn_x(PO_4)_3$/C samples using the XANES and their crystal structural evolution with XRD.

Fig. 4 represents the electrochemical kinetic properties of the fresh half-cells, assembled with selected samples as cathode materials. The intercept at the Z' axis in high frequency corresponds to uncompensated resistance (R_u) of the whole half-cells; the semicircle appears in middle frequency reflects the magnitude of charge transfer resistance (R_{ct}); the straight line in low frequency is attributed to the lithium-ion diffusion process (W) and capacitor nature of the samples due to the removal of the Li from the crystal lattice (C_{int}); what's more, the constant phase element (Q) was employed in the equivalent circuit (the inset lays in the lower right corner of Fig. 4) for the non-ideal capacitor characters of the double layer. Fitting results shows the increasing charge transfer resistances (*i.e.* 266.4, 470.6 and 532.5 Ω for the samples with the value of x = 0.00, 0.05, and 0.15, respectively), which may mean the decreasing electronic conductivities, accompanied with the increasing dopant amount. And the situation is not satisfied with our expectation, so more detailed studies are required to determine the correlation between the dopant and the electronic conductivities. What's a more, extensive study on the problem and potential solutions have been performed, and the details will be reported elsewhere, in which a most promising cathode material of $Li_3Zn_{0.05}V_{1.97}(PO_4)_3$/(C+PB) with ultra-long life and ultra-good rate performance are presented for lithium-capacitor ion batteries.

Now, let's go back and continue to focusing on the doping effects on the structural stability of LVP/C.

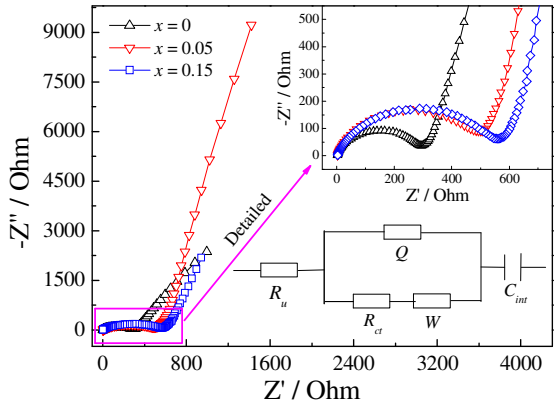

Fig.4 Nyquist plots of $Li_3V_{2-2/3x}Zn_x(PO_4)_3$/C ($x$ = 0, 0.05 and 0.15), and the inset lays in the lower right corner is the equivalent circuit used to fit the plots

XANES analyses

XANES was used to examine the effect of the zinc doping on the changes of oxidation states and the local environments of V elements in the compounds. V K-edge XANES spectra of $Li_3V_{2-2/3x}Zn_x(PO_4)_3$/C ($0 \leq x \leq 0.15$) are shown in Fig. 5. The main transition in the V K-edge involves the dipole transition of a V 1s electron to V 4p state with a weak pre-edge feature involving the non-dipole V 1s to 3d transitions. The main absorption edge of all pristine LVP/C samples, which is highlighted by the box in Fig.4a and enlarged as inset, appears at an energy that is close to that of V^{3+} (LVP used as vanadium 3+ standard) [30]. It is important to note the significant change in the pre-edge feature upon Zn doping (Fig. 5b). This pre-edge feature involves the non-dipole transition from V 1s to 3d state, which is shown to be sensitive to the vanadium oxidation state and the symmetry [30]. The low energy peak is more like V^{3+} with Oh symmetry and the higher one corresponds to V with higher oxidation and/or different geometry [31]. The reduced intensity of the second pre-edge peak (5469 eV) in Zn doped samples suggests that: 1) there is less V 3d and ligand p orbital hybridization, thus less distortion in the V-O Oh group, which may enhance the structural stability of LVP/C; 2) the less amount of more oxidized V that can be related to the increase of the capacity especially at higher charging plateau (4.3V); 3) the reduced V oxidation state in Zn doped samples suggests a higher V-O covalent bonding [32]. If this is true it will suggest a weaker P-O bond in doped samples *via* an inductive effect, and the following P L-edge results do support this interpretation very well.

P L-edge (Fig. 6) and Li K-edge (Fig. 7) XANES spectra are used to further understand Zn doping effect on LVP/C. Let us first focus on P L-edge XANES in Fig. 6, which involves mainly the P 2p to 3d dipole transitions. The resonant peak at 147 eV is the spectroscopic signature of PO_4^{3-} group and it is sensitive to P-O bond strength [32]. It is interesting to note that PO_4^{3-} peak of the 0.05 Zn doped sample shifted to lower energy (highlighted in Fig. 6a), relative to those of the other two samples, which could mean

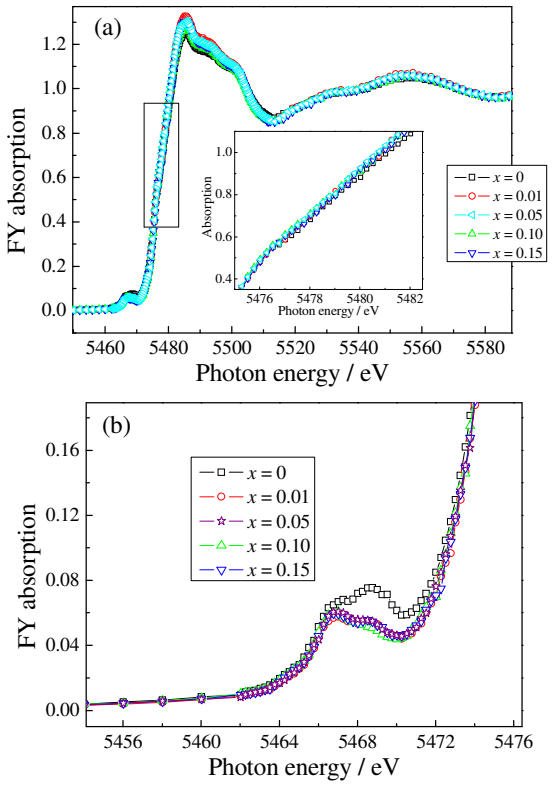

Fig.5 (a) XANES spectra of $Li_3V_{2-2/3x}Zn_x(PO_4)_3$/C samples at the V K-edge and (b) the corresponding pre-edge feature

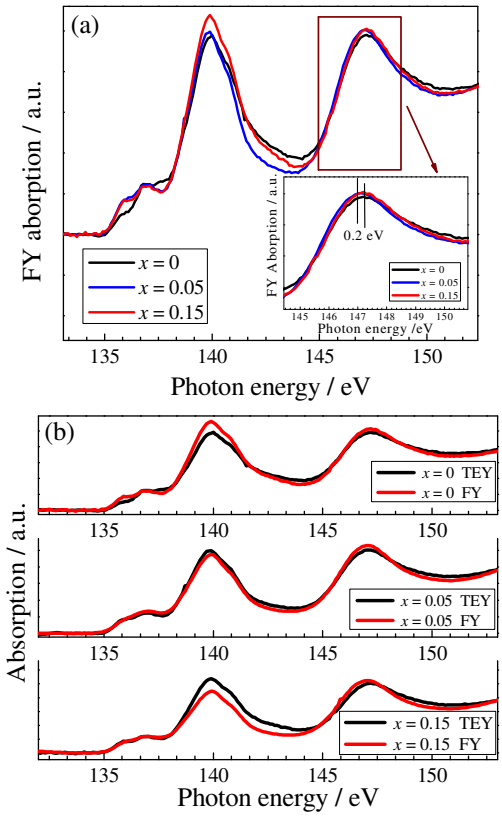

Fig.6 XANES spectra of $Li_3V_{2-2/3x}Zn_x(PO_4)_3$/C samples at the P L-edge recorded in (a) FY mode, and (b) shows the comparisons between TEY and FY modes

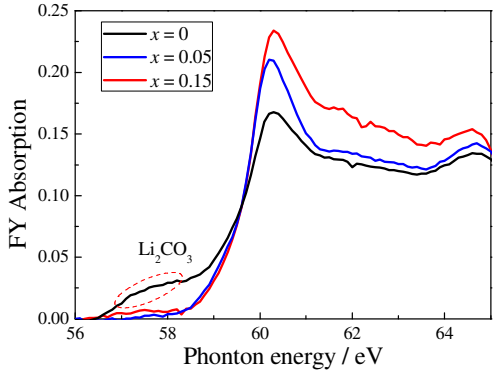

Fig.7 XANES spectra of $Li_3V_{2-2/3x}Zn_x(PO_4)_3$/C samples at the Li K-edge

a weaker P-O bond in the 0.05 Zn doped LVP. This is consistent with the assumption of a stronger V-O bonding based on observation of decrease in the pre-edge intensity at V K-edge XANES (Fig. 5). Furthermore, the comparison of TEY and FY P L-edge XANES at Fig. 6b shows that the surface sensitive TEY (~10 nm) and the bulk sensitive FY (~100 nm) spectra of 0.05 Zn doped LVP sample are almost the same, in contrast to those of the other two samples, which suggests that the 0.05 Zn doped sample has least surface and bulk difference. The difference observed in Fig. 6b for the higher Zn doping sample may be ascribed to the segregation of dopant to the surface, caused by heavy doping, as in the case of the semiconductor doping systems [33, 34]. It's worth noting that this segregation would detune the doping effect in this system, as it may limit the doping in the bulk level at high dopant concentrations. However, it should be note that the interesting phenomenon discovered can provide new clues to design materials with concentration gradient, like $LiNi_{1-x}M_xO_2$ presented in Ref. [35], for excellent electrochemical performance, due to the synergistic effect of certain features of each layer. And further understanding of segregation effect in cathode materials for LIBs, such LVP, may need more detailed studies. In regarding to the larger surface and bulk structure difference of the pristine LVP/C relative to 0.05 Zn doped LVP/C, the contamination of Li_2CO_3 are mainly responsible for the situation (as shown below in Li K-edge analysis).

The Li K-edge spectra of the pristine LVP/C and selected doped samples are shown in Fig. 7. First of all, the spectrum of the pristine LVP/C sample has a broad peak around 59 eV, assigned to Li_2CO_3 contamination [28] (may be formed during storage in the ambient [36]), which is absent in the spectra of the Zn doped samples. Furthermore, the Li K-edge spectrum of the 0.05 Zn doped sample has a sharper main peak around 60 eV, which could mean a stronger ionic Li bonding in this sample. Stronger ionic lithium would favor a faster diffusion of Li ion and shall contribute to the better electrochemical performance.

In summary, Zn doping has modified the local structure and composition of LVP, which shall help in delivering higher charge/discharge capacity. However, excess Zn doping ($x > 0.05$) will not only reduce the relative concentration of V, but also result dopant segregations. This could explain the optimized performance in the 0.05 Zn doped sample. Along with current XANES study on multiple elements and edges in Zn doped LVP, we also plan Zn K and L-edge XANES to directly probe Zn bonding environment to gain more insights on the structure

modification upon Zn doping.

Crystal structural evolution

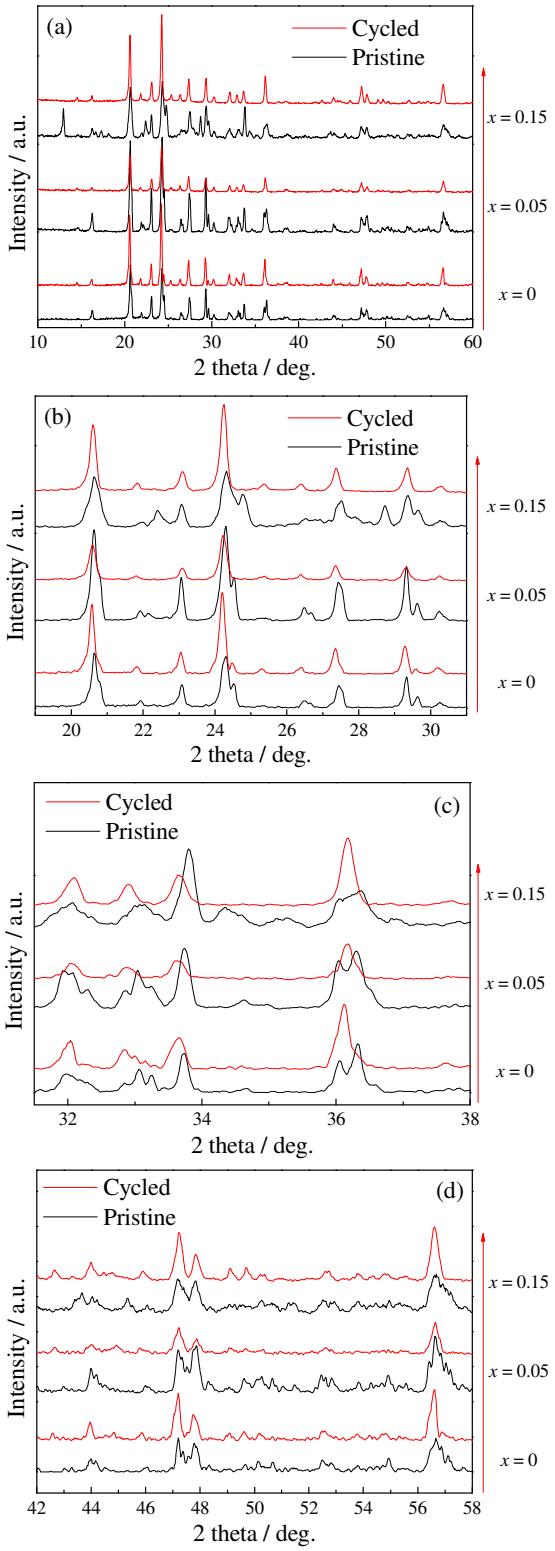

Fig.8 Comparison of XRD patterns of $Li_3V_{2-2/3x}Zn_x(PO_4)_3/C$ (x = 0, 0.05 and 0.15) before and after cycles. The comparison between $Li_3V_{2-2/3x}Zn_x(PO_4)_3/C$ (x = 0, 0.01 and 0.10) are provided in the supporting information

XRD analyses of $Li_3V_{2-2/3x}Zn_x(PO_4)_3/C$ (x = 0, 0.01, 0.15) were further performed in order to examine the long-term structural evolution upon repeated cycling. As shown in Fig. 8a, all diffraction peaks of the cycled samples can be indexed as monoclinic structure with a space group of 14($P2_1/n$). Careful observation of the XRD patterns (Fig. 8b-d) reveals that the diffraction peaks are systematically shifted to low angle, implying the increase in crystal plane inter-space [37, 38] and hence the lattice expansion caused by electrochemical cycling.

The lattice parameters of the selected samples and the corresponding cycled samples were obtained for further analyses. As can be seen from Table 3, the unit cell volumes and the value of c axis of all the selected samples enlarged upon repeated cycles, indicating that repeated extraction and reinsertion of lithium would finally cause the expansion of the crystal lattice. The degree of irreversible expansion of these two parameters was calculated and presented in Fig. 9. The irreversible of the c axis as well as the crystal volumes decrease markedly with the increase of the dopant amount. For x = 0.15, the irreversible expansion degree of the c axis and the unit cell volumes are 0.41% and 0.17%, respectively, indicating the highly reversibility of the sample, agreeing well with the cycling performance presented in Fig. 2b.

Table 3 Comparison of lattice parameters of $Li_3V_{2-2/3x}Zn_x(PO_4)_3/C$ (x = 0, 0.01 and 0.15) before and after cycles

Samples		a / nm	b / nm	c / nm	β	V / nm^3
0	Pristine	0.8634(8)	0.8592(2)	1.20446(6)	90.0564	0.8936(2)
	Cycled	0.8576(2)	0.8622(1)	1.21972(7)	90.0348	0.9019(2)
0.01	Pristine	0.8614(5)	0.8598(6)	1.21010(5)	90.2318	0.8963(5)
	Cycled	0.8602(4)	0.8614(6)	1.21891(3)	90.0902	0.9032(9)
0.05	Pristine	0.8627(0)	0.8602(0)	1.20952(7)	90.3018	0.8975(8)
	Cycled	0.8611(8)	0.8617(7)	12.1613(6)	90.5854	0.9024(9)
0.10	Pristine	0.8620(8)	0.8611(8)	1.21094(2)	90.0266	0.8990(1)
	Cycled	0.8604(9)	0.8611(0)	1.2168(2)	90.2301	0.9016(2)
0.15	Pristine	0.8634(1)	0.8589(2)	1.21356(4)	90.3162	0.8999(7)
	Cycled	0.8595(7)	0.8606(6)	1.21857(4)	89.8445	0.9015(0)

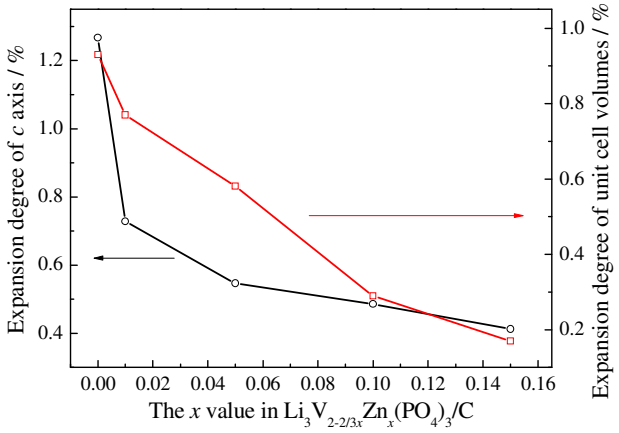

Fig.9 The effect of the doping amount of zinc on the irreversible expansion degree of c axis and unit cell volumes

In summary, the Zn doping is believed not only to enhance the

structural stability of the pristine LVP/C, but also to prevent the irreversible expansion of the crystal lattice upon repeated cycles, thus enhance the cycle performance.

Conclusions

Pristine and zinc doped $Li_3V_2(PO_4)_3$/C were prepared *via* carbon thermal reduction method coupled with a ball-mill process. It is shown that a suitable amount ($0 < x \leq 0.15$) of zinc doping can enhance the cycling performance by stabilizing the crystal structure of the samples, as confirmed by structural change revealed by the V K-edge, P L-edge and Li K-edge XANES results as well as the decreasing irreversible expansion degree of the *c* axis and the unit cell volumes upon repeated cycles as revealed by the XRD. In addition to the enhanced crystal structure stability, the reduced particle size and the formation of the spherical morphology accompany with the suitable amount (x = 0.05) of zinc doping are also key to improving the electrochemical performance. Due to comprehensive effects of the aforementioned factors, $Li_3V_{1.97}Zn_{0.05}(PO_4)_3$/C shows the best electrochemical performance in $Li_3V_{2-2/3x}Zn_x(PO_4)_3$/C series.

Acknowledgment

This work was supported by the National Natural Science Foundation of China (no. 51274075), the National Environmental Technology Special Project (no. 201009028), and Guangdong Province-department University-industry Collaboration Project (grant nos. 2012B091100315). CLS is supported by NSERC, NRC, CIHR and the University of Saskatchewan.

Wenhui Wang is now futher his study in the Chinese University of Hong Kong.

Notes and references

[a] *Harbin Institute of Technology, School of Chemical Engineering and Technology, Xidazhi Street, 150001 Harbin, China.Fax:86 451 86413721; Tel: 86 451 86413751; E-mail: changsd@hit.edu.cn*
[b] *Canadian Light Source Inc., University of Saskatchewan, Saskatoon, SKS7N2V3*
† These authors contributed equally to this work.

1 X.S. Liu, J. Liu, R.M. Qiao, Y. Yu, H. Li, L.M. Suo, Y.S.g Hu, Y.D. Chuang, G.J. Shu, F.C.a Chou, T.C. Weng, D. Nordlund, D. Sokaras, Y.J. Wang, H. Lin, B. Barbiellini, A. Bansil, X.Y. Song, Z. Liu, S.S. Yan, G. Liu, S. Qiao, T.J. Richardson, D. Prendergast, Z. Hussain, F.M.F. de Groot and W.L. Yang, *J. Am. Chem. Soc.* 2012, **134**, 13708.
2 L.S. Cahill, R.P. Chapman, J.F. Britten and G.R. Goward, *J. Phys. Chem. B* 2006, **110**, 7171.
3 S.C. Yin, H. Grondey, P. Strobel, H. Huang and L.F. Nazar, *J. Am. Chem. Soc.* 2003, **125**, 326.
4 S.C. Yin, H. Grondey, P. Strobel, M. Anne and L.F. Nazar, *J. Am. Chem. Soc.* 2003, **125**, 10402.
5 H. Huang, S.C. Yin, T. Kerr, N. Taylor and L.F. Nazar, *Adv. Mater.* 2002, **14**, 1525.
6 L. Wang, L.C. Zhang, I. Lieberwirth, H.W. Xu and C.H. Chen, *Electrochem. Commun.* 2010, **12**, 52.
7 Z.Y. Chen, C.S. Dai, G. Wu, M. Nelson, X.G. Hu, R.X. Zhang, J.S. Liu and J.C. Xia, *Electrochim. Acta* 2010, **55**, 8595.
8 L.L. Zhang, G. Liang, G. Peng, Y.H. Huang, L. Wang, L. Qie, M.C. Croft, A. Ignatov and J.B. Goodenough, *J. Electrochem. Soc.* 2010, **159**, A1573.
9 A.Q. Pan, J. Liu, J.G. Zhang, W. Xu, G.Z. Cao, Z.M. Nie, B.W. Arey and S.Q. Liang, *Electrochem. Commun.* 2010, **12**, 1674.
10 H.D. Liu, G. Yang, X.F. Zhang, P. Gao, L. Wang, J.H. Fang, J. Pinto and X.F. Jiang, *J. Mater. Chem.* 2012, **22**, 11039.
11 L.L. Zhang, G. Liang, G. Peng, F. Zou, Y.H. Huang, M.C. Croft, A. Ignatov, *J. Phys. Chem. C* 2012, **116**, 12401.
12 L. Zhang, X.L. Wang, J.Y. Xiang, Y. Zhou, S.J. Shi and J.P. Tu, *J. Power Sources* 2010, **195**, 5057.
13 X.H. Rui, C. Li, J. Liu, T. Cheng and C.H. Chen, *Electrochim. Acta* 2010, **55**, 6761.
14 H.W. Liu, C.X. Cheng, X.T. Huang and J.L. Li, *Electrochim Acta* 2010, **55**, 8461.
15 A.Q. Pan, D.W. Choi, J.G. Zhang, S.Q. Liang, G.Z. Cao, Z.M. Nie, B.W. Arey and J. Liu, *J. Power Sources* 2011, **196**, 3646.
16 Y.Q. Qiao, X.L. Wang, Y.J. Mai, J.Y. Xiang, D. Zhang, C.D. Gu and J.P. Tu, *J. Power Sources* 2011, **196**, 8706.
17 L.L. Zhang, G. Peng, G. Liang, P.C. Zhang, Z.H. Wang, Y. Jiang, Y.H. Huang and H. Lin, *Electrochim. Acta* 2013, **90**, 433.
18 Y. Xia, W.K. Zhang, H. Huang, Y.P. Gan, C.G. Li and X.Y. Tao, *Mater. Sci. Eng. B* 2011, **176**, 633.
19 M.M. Ren, Z. Zhou, Y.Z. Li, X.P. Gao and J. Yan, *J. Power Sources* 2006, **162**, 1357.
20 D.J. Ai, K.Y. Liu, Z.G. Lu, M.M. Zou, D.Q. Zeng and J. Ma, *Electrochim. Acta* 2011, **56**, 2823.
21 Y.G. Mateyshina and N.F. Uvarov, *J. Power Sources* 2011, **196**, 1494.
22 C.W. Sun, S. Rajasekhara, Y.Z. Dong and J.B. Goodenough, *ACS Appl. Mater. Interfaces* 2011, 3, 3772.
23 W.H. Wang, Z.Y. Chen, J.L. Zhang, C.S. Dai, J.J. Li and D.L. Ji, *Electrochim. Acta* 2013, 103, 259.
24 J.N. Son, S.H. Kim, M.C. Kim, G.J. Kim, V. Aravindan, Y.G. Lee and Y.S. Lee, *Electrochim. Acta* 2013, **97**, 210.
25 J.B. Goodenough, Y. Kim, *Chem. Mater.* 2010, **22**, 587.
26 H. Liu, Q. Cao, L.J. Fu, C. Li, Y.P. Wu and H.Q. Wu, *Electrochem. Commun.* 2006, **8**, 1553.
27 A.Y. Shenouda and H.K. Liu, *J. Alloy. Compd.* 2009, **477**, 498.
28 S.L. Yang, D.N. Wang, G.X. Liang, Y.M. Yiu, J.J. Wang, L.J. Liu, X.L. Sun and T.K. Sham, *Energy Environ. Sci.* 2012, **5**, 7007.
29 J.R. Croy, M. Balasubramanian, D.H. Kim, S.H. Kang and M.M. Thackeray, *Chem. Mater.* 2011, **23**, 5415.
30 F. Omenya, N.A. Chernova, S. Upreti, P.Y. Zavalij, K.W. Nam, X.Q. Yang and M.S. Whittingham, *Chem. Mater.* 2011, **23**, 4733.
31 P. Chaurand, J. Rose, V. Briois, M. Salome, O. Proux, V. Nassif, L. Olivi, J. Susini, J.L. Hazemann and J.Y. Bottero, *J. Phys. Chem. B* 2007, **111**, 5101.
32 J.G. Zhou, J. Wang, L. Zuin, T. Regier, Y.F. Hu, H.L. Wang, Y.Y. Liang, J. Maley, R. Sammynaiken and H.J. Dai, *Phys. Chem. Chem. Phys.* 2012, **14**, 9578.
33 Z.J. Qiu, Z. Zhang, Mi. Östling and S.L. Zhang, *IEEE T. Electron Dev.* 2008, **55**, 396.
34 R. Janisch, P. Gopal and N.A. Spaldin, *J. Phys.-Condens. Mat.* 2005, **17**, R657.
35 Y.K. Sun, S.T. Myung, B.C. Park, J. Prakash, I. Belharouak and K. Amine, *Nat. Mater.* 2009, **8**, 320.
36 J.G. Zhou, H.T. Fang, J.M. Maley, M.W. Murphy, J.Y. Peter Ko, J.N. Cutler, R. Sammynaiken, T.K. Sham, M. Liu and F. Li, *J. Mater. Chem.* 2009, **19**, 6804.
37 J.S. Wark, R.R. Whitlock, A.A. Hauer, J.E. Swain, P.J. Solone, *Phys. Rev. B* 1989, **40**, 5705.
38 S.S.P. Parkin, V.Y. Lee, A.I. Nazzal, R. Savoy, T.C. Huang, G. Gorman and R. Beyers, *Phys. Rev. B* 1988, **38**, 6531.